Fabrication and measurements of superconducting flux qubits at RHUL

T. Hoenigl-Decrinis, A. Dmitriev, R. S. Shaikhaidarov, V. N. Antonov, O. V. Astafiev

We successfully fabricated and characterized superconducting flux qubits coupled to an open 1D space by means of resonance fluorescence and studied its dynamics by measuring evolutions of its coherent and incoherent emission. The qubit can be considered as an artificial atom with controllable parameters. We observe strong interaction of the artificial atom with the electromagnetic field, which can result in 99% extinction of propagating waves. Furthermore, states of the atom were fully controllable by resonant excitation microwave pulses. This allows applications of controllable artificial atoms in quantum optics and photonics.

Device Fabrication.

The flux qubits have been fabricated in the cleanroom facilities at the Royal Holloway Physics Department. A scanning-electron micrograph of the device is presented in Fig. 1.

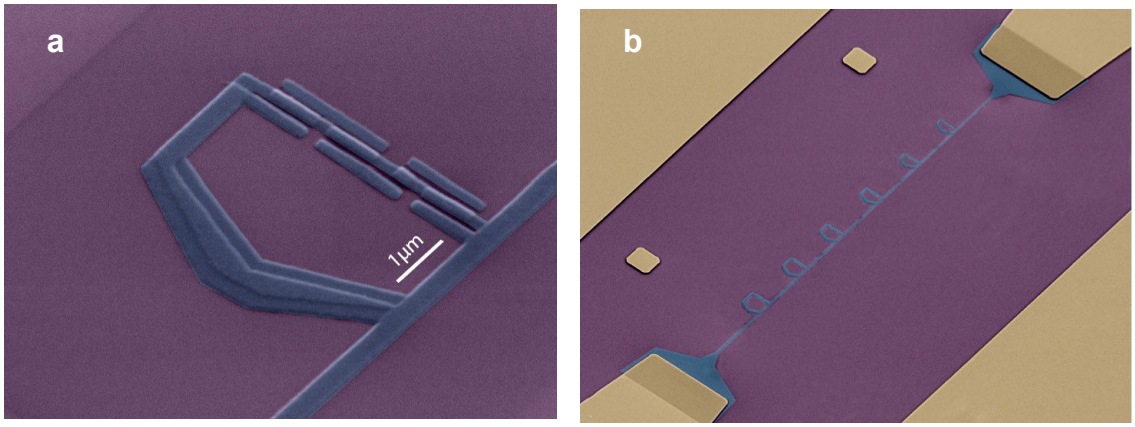

Figure 1: (a) False-colored scanning-electron micrograph (SEM) of a flux qubit coupled to a 1D transmission line. The flux qubit consists of a macroscopic superconducting loop interrupted by four Josephson junctions that are inductively coupled to the line. **(b)** Six flux qubits with varying loop area inductively coupled to the transmission line. Colour-code: Yellow, blue, and violet correspond to gold, aluminum and the substrate respectively.

Our flux qubits are superconducting loops interrupted by four Josephson junctions (JJ) [1]. Three JJs are identical to each other, while the fourth one has a reduced size by a factor of 0.5. The qubits are fabricated by

means of electron-beam lithography and the film is deposited using shadow evaporation technique with oxidation. There are 6 qubits coupled to the transmission line in each experimental sample.

The coplanar transmission line with a characteristic impedance Z = 50 Ω is made by patterning a gold film on a silicon substrate. In the middle of the chip, the central conductor of the waveguide is narrowed and replaced by aluminium. The latter is deposited together with the qubits using shadow evaporation. The experiment is performed in a dilution refrigerator at a temperature of about 15 mK.

Theoretical background

In order to understand the behavior of a qubit as an artificial atom, discussion of the relevant theory is required. The loops, interrupted by Josephson junctions (identical to a flux qubit [1]) and threaded by a bias flux Φ_b close to a half flux quantum $\Phi_0/2$, shares a segment with the transmission line, which results in a loop-line mutual inductance *M* mainly due to kinetic inductance of the shared segment [2]. The two lowest eigenstates of the atom are naturally expressed via superpositions of two states with persistent current, I_p, flowing clockwise or counterclockwise. In the energy eigenbasis, the lowest two levels $|g\rangle$ and $|e\rangle$ are described by the truncated Hamiltonian $H = \hbar\omega_a\sigma_z/2$, where $\omega_a = \sqrt{\omega_0^2 + \varepsilon^2}$ is the atomic transition frequency and σ_i $(i = x, y, z)$ are the Pauli matrices. Here, $\hbar\varepsilon = 2I_p\delta\Phi$ ($\delta\Phi \equiv \Phi_b - \Phi_0/2$) is the energy bias controlled by the bias flux, and $\hbar\omega_0$ is the anticrossing energy between the two persistent current states. The excitation energies of the third and higher eigenstates are much larger than $\hbar\omega_a$; therefore they can be neglected in this analysis.

We consider a dipole interaction of the atom with a field of an electromagnetic 1D wave. In the semiclassical approach of quantum optics, the external field of the incident wave $I_0(x,t) = I_0 e^{ikx - i\omega t}$ (here ω is the frequency and *k* is the wavenumber) induces the atomic polarization. The atom with characteristic loop size ~ 10 μm (negligibly small compared to the

wavelength $\lambda \sim 1$ cm) placed at $x = 0$ generates scattered waves $I_{sc}(x,t) = I_{sc}e^{ik|x|-i\omega t}$, propagating in both directions, forward and backward. The current oscillating in the loop under the external drive induces an effective magnetic flux ϕ, playing a role of atomic polarization. The net wave $I(x,t) = (I_0 e^{ikx} + I_{sc}e^{ik|x|})e^{-i\omega t}$ satisfies the 1D wave equation $\partial_{xx} I - v^{-2}\partial_{tt} I = c\delta(x)\partial_{tt}\phi$, where the wave phase velocity is $v = 1/\sqrt{lc}$ (l and c are inductance and capacitance per unit length) and the dispersion relation is $\omega = vk$.

At the degeneracy point, when $\varepsilon = 0$ and $\omega_a = \omega_0$, the dipole interaction of the atom with the electromagnetic wave in the transmission line is $H_{int} = -\phi_p \mathrm{Re}[I_0(0,t)]\sigma_x$, where the dipole moment matrix element $\phi_p = MI_p$. Then in the rotating wave approximation, the standard form of the Hamiltonian of a two-level atom interacting with the nearly resonant external field is

$$H = -\frac{\hbar\delta\omega}{2}\sigma_z - \frac{\hbar\Omega}{2}\sigma_x \tag{1}$$

Here $\delta\omega = \omega - \omega_0$ is the detuning and $\hbar\Omega = \phi_p I_0$ is the dipole interaction energy. The time-dependent atomic dipole moment can be presented for a negative frequency component as $\langle\phi(t)\rangle = \phi_p\langle\sigma^-\rangle e^{-i\omega t}$, and the boundary condition for the scattered wave generated due to the atomic polarization satisfies the equation $2ik(I_{sc}/2) = -\omega^2 c\phi_p\langle\sigma^-\rangle$, where $\sigma^{\pm} = (\sigma_x \pm i\sigma_y)/2$. Assuming that the relaxation of the atom is caused solely by the quantum noise of the open line, we obtain the relaxation rate $\Gamma_1 = (\hbar\omega\phi_p^2)/(\hbar^2 Z)$ (here $Z = \sqrt{l/c}$ is the line impedance) and find

$$I_{sc}(x,t) = i\frac{\hbar\Gamma_1}{\phi_p}\langle\sigma^-\rangle e^{ik|x|-i\omega t}. \tag{2}$$

This expression indicates that the atomic dissipation into the line reveals itself even in elastic scattering.

Due to this dissipation further analysis of the evolution of the density matrix is required. The atom coupled to the open line is described by the

density matrix ρ, which satisfies the master equation $\dot{\rho} = -\frac{i}{\hbar}[H, \rho] + \hat{L}[\rho]$. At zero temperature, the simplest form of the Lindblad operator $\hat{L}[\rho] = -\Gamma_1 \sigma_z \rho_e - \Gamma_2(\sigma^+ \rho_{eg} + \sigma^- \rho_{ge})$ describes energy relaxation (the first term) and the damping of the off-diagonal elements of the density matrix with the dephasing rate $\Gamma_2 = \Gamma_1/2 + \Gamma_\varphi$, where Γ_φ is the pure dephasing rates. It is convenient to define reflection and transmission coefficients r and t according to $I_{sc} = -rI_0$ and $I_0 + I_{sc} = tI_0$, and, therefore, $t = 1 - r$. From Eq. 2 we find the stationary solution

$$r = r_0 \frac{1 + i\delta\omega/\Gamma_2}{1 + (\delta\omega/\Gamma_2)^2 + \Omega^2/\Gamma_1\Gamma_2}, \tag{3}$$

where the maximal reflection amplitude $r_0 = \eta\Gamma_1/2\Gamma_2$ at $\delta\omega = 0$. Here η presents dimensionless coupling efficiency to the line field, including non-radiative relaxation. The maximal possible power extinction $(1 - |t|^2)$ can reach 100% when $|r_0| = 1$. It takes place for $\eta = 1$ and $\Gamma_2 = \Gamma_1/2$, that is, in the absence of pure dephasing, $\Gamma_\varphi = 0$. In such case, the wave scattered forward by the atom is canceled out due to destructive interference with the incident wave, $I_{sc} = -I_0$. Note that although Eq. 3 is obtained for the degeneracy point when $\varepsilon = 0$, it remains valid in the general case of $\varepsilon \neq 0$ if the dipole interaction energy $\hbar\Omega$ is multiplied by ω_0/ω_a.

Transmission Spectroscopy

The excitation energy of the atom is revealed by transmission spectroscopy (Fig. 2). Owing to the broadband characteristics of the transmission line, we are able to sweep the frequency of the incident microwave in a wide range and monitor the transmission. We detect three out of the six qubits with the remaining three being out of our measurement range. Note that the wide range of the energies has been chosen on purpose for optimisation of our fabrication parameters. We observe the systematic change of the energies according to our expectations, which indicates a 100% fabrication yield.

As shown in Fig. 3, the resonance reveals itself as a sharp dip in the power transmission coefficient $|t|^2$. At resonance, the power extinction reaches its maximal value of 99%, which suggests that the system is well isolated from other degrees of freedom in the surrounding solid state environment and behaves as an isolated atom in open space, coupled only to the electromagnetic fields in the space. The resonance frequency ω_a is traced as a function of the flux bias $\delta\Phi$. By fitting the data, we obtain for the three qubits $\omega_0/2\pi = 2.450$ GHz, 5.216 GHz and 14.678 GHz at $\delta\Phi = 0$ (the degeneracy points), and the persistent current, $I_p = 465$ nA, $I_p = 416$ nA and $I_p = 273$ nA respectively

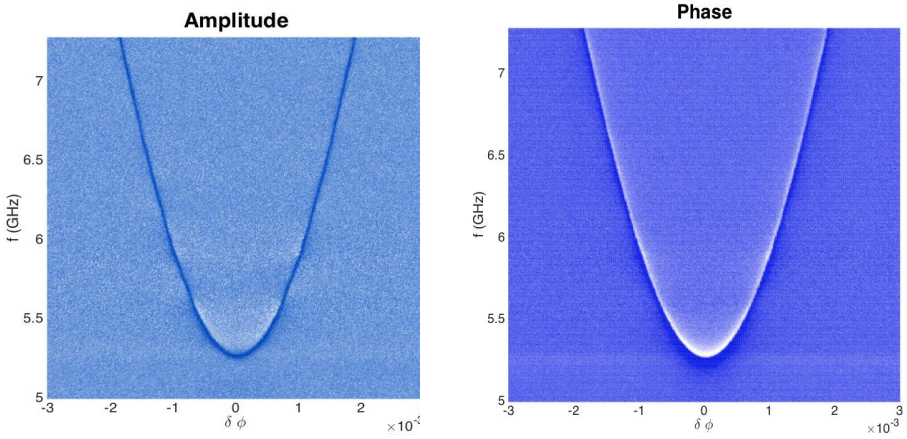

Figure 2: Qubit Spectroscopy. Power transmission coefficient $|t|^2$ as a function of flux bias, $\delta\Phi$, and incident microwave frequency, *f*.

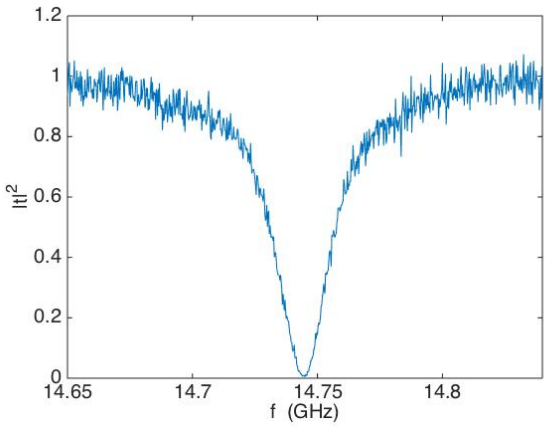

Figure 3: Power transmission coefficient at $\delta\Phi = 0$ versus incident wave detuning $\delta\omega/2\pi$ from the resonance frequency $\omega_0/2\pi = 14.678$ GHz with a driving power of −28dBm. The maximal power extinction of 99% occurs at resonance.

Mollow triplet

So far we have investigated elastic Rayleigh scattering in which the incident and the scattered waves have the same frequency. However, the rest of the power $W'_{sc} = W_0\left(1-|t|^2-|r|^2\right)$ is scattered inelastically and can be observed in the power spectrum. Figure 4 shows the spectrum measured at the degeneracy point ($\delta\Phi = 0$) at fixed driving powers. It manifests the resonance fluorescence triplet, also known as the Mollow triplet.

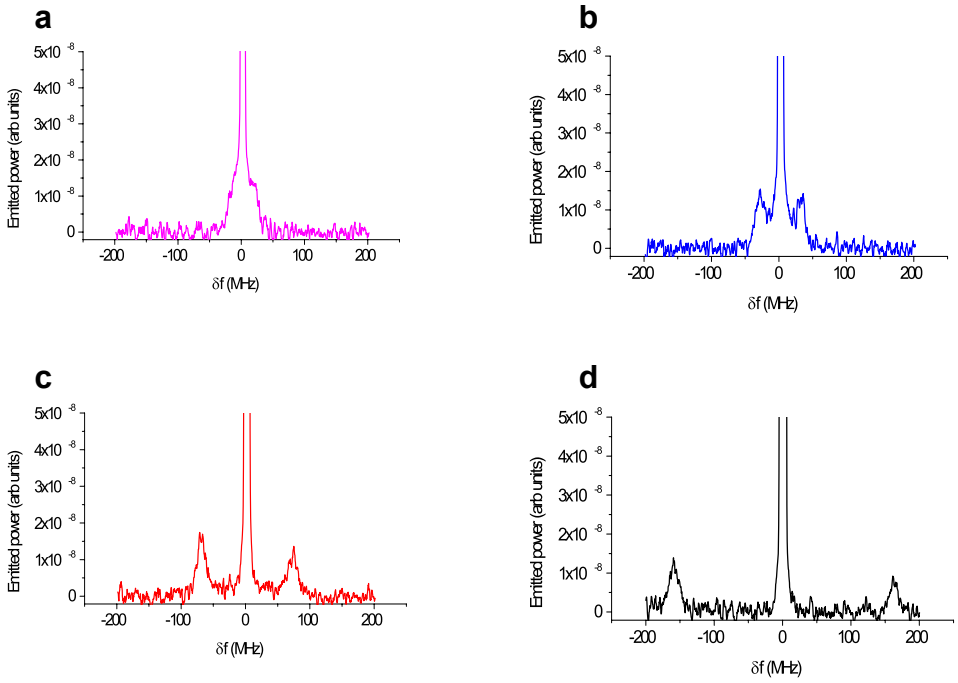

Figure 4: The Mollow Triplet: Spectrum measured at the degeneracy point ($\delta\Phi = 0$) under a resonant drive with the power corresponding to **(a)** -30dBm, **(b)** -15dBm, **(c)** -10dBm, and
(d) 0dBm.

In the case of a strong driving field ($\Omega^2 >> \Gamma_1^2$), the expression for the inelastically scattered power simplifies to $W'_{sc} \approx \left(\Gamma_1^2/\Omega^2\right)W_0$, which is independent of the incident power and can be rewritten as $W'_{sc} \approx \hbar\omega\Gamma_1/2$: The atom is half populated by the strong drive and spontaneously emits with rate Γ_1 . Assuming $\eta = 1$, the spectral density measured in one of the two directions is expected to be

$$S(\omega) \approx \frac{1}{2\pi}\frac{\hbar\omega\Gamma_1}{8}\left(\frac{\gamma_s}{(\delta\omega+\Omega)^2+\gamma_s^2}+\frac{2\gamma_c}{\delta\omega^2+\gamma_c^2}+\frac{\gamma_s}{(\delta\omega-\Omega)^2+\gamma_s^2}\right), \qquad (4)$$

where half-width of the central and side peaks are $\gamma_c = \Gamma_2$ and $\gamma_s = (\Gamma_1 + \Gamma_2)/2$. Our results are in good agreement with the theory indicating high collection efficiency of the emitted photons due to the 1D confinement of the mode. The shift of the side peaks, $\pm\Omega$, from the main resonance depends on the driving power. The intensity plot in Fig. 5 shows how the resonance fluorescence emission depends on the driving power.

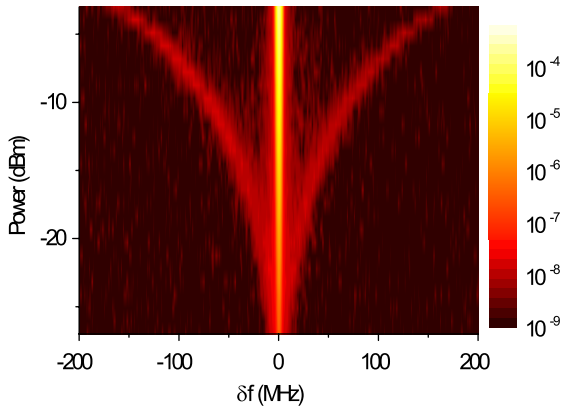

Figure 5: Resonance fluorescence emission spectrum as a function of the driving power.

Observation of quantum oscillation

Finally, we have studied the dynamics of the artificial two-level atom in an open 1D space by measuring evolution of its coherent and incoherent emission.

The qubit states are fully controllable by resonant excitation microwave pulses. The coherent emission – a direct measure of superposition in the atom – exhibits decaying oscillations shifted by $\pi/2$ from oscillations of the incoherent emission, which, in turn, is proportional to the atomic population. The emission dynamics provides information about states and properties of the atom.

Manipulating the atomic states by microwave pulses, one can perform the quantum state and process tomography. The excited atom is a dynamical system, which continuously emits radiation to the line, similarly to natural atoms in the open space. However differently from the optical measurements of the natural atoms, the collection efficiency of the emission to the 1D

transmission line by the artificial atom is very high due to its strong coupling [3].

The dynamics of such a system is described similarly to a spin-1/2 in the magnetic field and is governed by the optical Bloch equations $\frac{d\vec{\sigma}}{dt} = \boldsymbol{B}\vec{\sigma} + \vec{b}$, where

$$B = \begin{pmatrix} -\Gamma_2 & 0 & -\Omega\sin\varphi \\ 0 & -\Gamma_2 & -\Omega\cos\varphi \\ \Omega\sin\varphi & \Omega\cos\varphi & -\Gamma_1 \end{pmatrix} \quad (5)$$

$\vec{b} = \{0,0,-\Gamma_1\}$, and $\vec{\sigma} = \{\langle\sigma_x\rangle, \langle\sigma_y\rangle, \langle\sigma_z\rangle\}$ is a vector of the expectation values of the Pauli matrices. This vector represents the atomic state, accounting incoherent processes of relaxation with the rate Γ_1, decay of z-component, and dephasing with the rate $\Gamma_2 = \gamma + \Gamma_1/2$,decay in xy-plane, where γ is the pure dephasing rate. In the Rabi rotation, the phase ϕ controls the axis; e.g., $\varphi = 0$ and $\varphi = \pi/2$ cause the spin rotations around x- and y- axes, respectively. Combining pulses with different φ, one can controllably rotate the spin, while $|\vec{\sigma}| < 1|$ subjected to the incoherent processes.

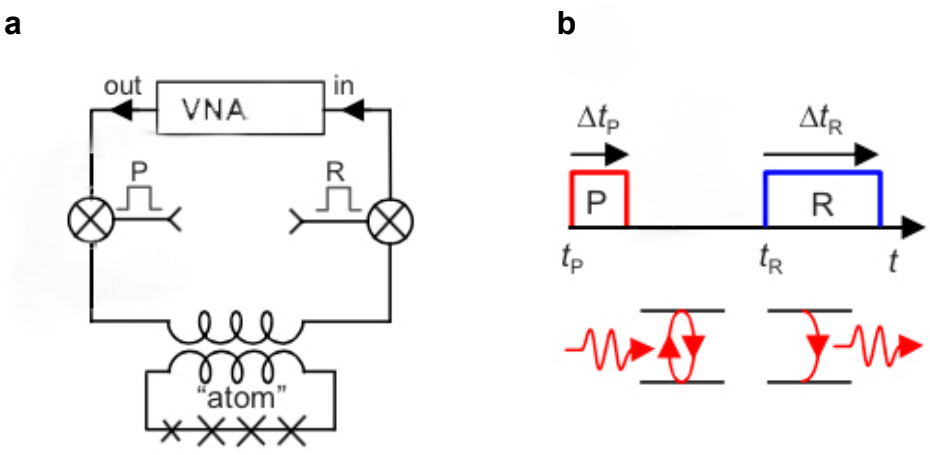

Figure 6: **(a)** Measurement circuit diagram. **(b)** General pulse sequence (upper panel) with schematic atomic dynamics (lower panel): The driving pulse P is used to prepare the atomic states, and the emission from the atom is detected during the readout pulse R.

A schematic diagram of the measurement setup is presented in Fig. 6(a). We prepare the atom in a mixed state by one microwave pulse (denoted by P) of lengths Δt_P applied at times t_P. A continuous microwave is chopped by the rectangular pulse P with the chopper consisting of a high-frequency mixer. The signal is delivered to the sample in a dilution refrigerator (at T ≈ 15 mK) through a coaxial cable. The output signal is amplified by a cryogenic amplifier and a room-temperature amplifier. The signal is detected by a vector network analyzer (VNA) in the homodyne measurement of the coherent emission. Coherent and incoherent dynamics of the system is studied by measuring the emission from the atom. A single microwave pulse P of varied length Δt_P is applied to the atom with the readout pulse R following right after P as illustrated in Fig. 6 (b).

Figure 7 shows the coherent dipole emission measured by the VNA, which is directly proportional to $\langle \sigma^- \rangle$. The oscillations decay, while the emission saturates to a finite stationary level defined by $\langle i\sigma^- \rangle = (\Gamma_1\Omega/2)/(\Gamma_1\Gamma_2 + \Omega^2)$ ($\equiv \langle \sigma_y \rangle/2$) [4]. The emission at different driving powers is exemplified in Fig. 7(a).

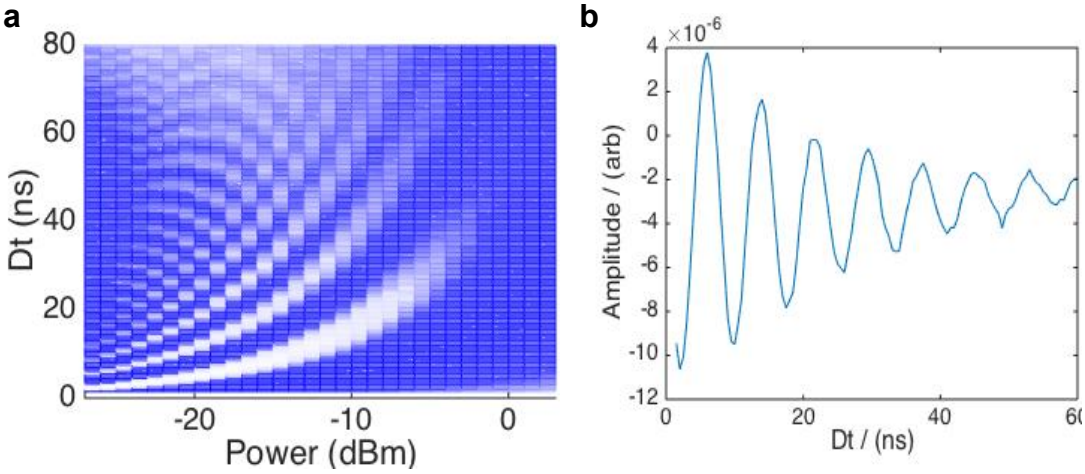

Figure 7: Rabi Oscillations. **(a)** Intensity plot of quantum oscillations as a function of driving power and delay time. **(b)** Evolution of the amplitude of coherent emission from our 2-level system at a fixed driving power of -6dBm.

References

[1] J.E. Mooij, T. P. Orlando, L. Levitov, L. Tian, C. H. van der Wal, and S. Loyld, Science 285, 1036 (1999).

[2] A. A. Abdumalikov, O. Astafiev, Y. Nakamura, Y. A. Pashkin, and J.-S. Tsai, Phys. Rev. B 78, 180502(R)(2008).

[3] O. Astafiev, A. M. Zagoskin, A. A. Abdumalikov Jr., Yu. A. Pashkin, T. Yamamoto, K. Inomata, Y. Nakamura, and J.S. Tsai, Science 327, 840 (2010).

[4] A. A. Abdumalikov, Jr., O. V. Astafiev, Yu. A. Pashkin, Y. Nakamura, and J. S. Tsai, Phys. Rev. Lett. 107, 043604 (2011)